2023-05-15

Ocean acidification stunts molluscan growth at CO2 seeps

Zhao, L

10.1016/j.scitotenv.2023.162293
Science of The Total Environment
Elsevier BV

Ocean acidification stunts molluscan growth at CO_2 seeps

Liqiang Zhao [a, b, *], Ben P. Harvey [c, *], Tomihiko Higuchi [b], Sylvain Agostini [c], Kentaro Tanaka [b], Naoko Murakami-Sugihara [b], Holly Morgan [d], Phoebe Baker [d], Jason M. Hall-Spencer [c, d], Kotaro Shirai [b]

[a] *College of Fisheries, Guangdong Ocean University, Zhanjiang 524088, China*

[b] *Atmosphere and Ocean Research Institute, The University of Tokyo, Chiba 277-8564, Japan*

[c] *Shimoda Marine Research Center, University of Tsukuba, Shimoda 415-0025, Japan*

[d] *School of Biological and Marine Sciences, University of Plymouth, Plymouth PL4 8AA, UK*

***** *Co-corresponding authors*:

lzhao@gdou.edu.cn (L.Z.); ben.harvey@shimoda.tsukuba.ac.jp (B.P.H.)

Abstract

Ocean acidification can severely affect bivalve molluscs, especially their shell calcification. Assessing the fate of this vulnerable group in a rapidly acidifying ocean is therefore a pressing challenge. Volcanic CO_2 seeps are natural analogues of future ocean conditions that offer unique insights into the scope of marine bivalves to cope with acidification. Here, we used a 2-month reciprocal transplantation of the coastal mussel *Septifer bilocularis* collected from reference and elevated pCO_2 habitats to explore how they calcify and grow at CO_2 seeps on the Pacific coast of Japan. We found significant decreases in condition index (an indication of tissue energy reserves) and shell growth of mussels living under elevated pCO_2 conditions. These negative responses in their physiological performance under acidified conditions were closely associated with changes in their food sources (shown by changes to the soft tissue $\delta^{13}C$ and $\delta^{15}N$ ratios) and changes in their calcifying fluid carbonate chemistry (based on shell carbonate isotopic and elemental signatures). The reduced shell growth rate during the transplantation experiment was further supported by shell $\delta^{13}C$ records along their incremental growth layers, as well as their smaller shell size despite being of comparable ontogenetic ages (5-7 years old, based on shell $\delta^{18}O$ records). Taken together, these findings demonstrate how ocean acidification at CO_2 seeps affects mussel growth and reveal that lowered shell growth helps them survive stressful conditions.

Keywords: Climate change; Bivalves; Calcification; Acclimation; Sclerochronology

1. Introduction

Since the Industrial Revolution, the atmospheric concentration of carbon dioxide (CO_2) has increased at an unprecedented rate from about 280 ppm in 1750 to 410 ppm in 2018, due mainly to human activities such as burning fossil fuels (Blunden et al., 2018). About one-third of all anthropogenic CO_2 has entered the ocean, causing decreases in seawater pH, carbonate ion (CO_3^{2-}) concentration, and saturation state of calcium carbonate ($CaCO_3$), and increases in the partial pressure of CO_2 (pCO_2) and bicarbonate ion (HCO_3^-) concentration (Caldeira and Wickett, 2003). These fundamental changes in seawater chemistry, known as ocean acidification (OA), can severely affect most marine bivalves, one of the most ecologically and economically important taxonomic groups in global marine ecosystems (e.g., Ekstrom et al., 2015; Leung et al., 2020a; Melzner et al., 2020; Martins et al. 2021; Leung et al., 2022). In particular, the ability of marine bivalves to calcify, which in turn controls individual growth, development, defense and survival, is highly sensitive to CO_2-driven changes in seawater carbonate system (e.g., Waldbusser et al., 2014; Thomsen et al., 2017; Zhao et al., 2017a; Rajan et al., 2021). Hence, obtaining an integrated understanding of how OA affects the calcification physiology can represent an important step forward in assessing the fate of marine bivalves in a rapidly acidifying ocean.

The calcification of marine bivalves can be thought of as a step-by-step process, and OA can likely affect each of these separate steps. This includes OA substantially affecting the source and pathway of calcifying substrates such as Ca^{2+} and HCO_3^- ions

transported from ambient seawater to the calcifying front (Lu et al., 2018; Sillanpää et al., 2018; Zhao et al., 2018a), and the removal of protons generated during the $CaCO_3$ precipitation (Zhao et al., 2017b; Liu et al., 2020). Likewise, the synthesis of organic matrix for the $CaCO_3$ crystallization and periostracum formation can succumb under acidified conditions (Hüning et al., 2013; Ramajo et al., 2016). Nevertheless, continuous *in situ* monitoring of changes at the calcifying front remains an extremely challenging task, due to the thin extrapallial space located between the inner shell layer and mantle tissue (Marin et al., 2012; He et al., 2023). Alternatively, a suite of geochemical proxies archived in shell carbonates hold great potential for estimating responses to ocean acidification (Levin et al., 2015). When exposed to elevated pCO_2, for example, the relative contribution of seawater carbon and metabolic carbon to the calcifying pool can be examined by shell carbon isotopes (Lu et al., 2018; Zhao et al., 2018a). The amount of boron and uranium incorporated into shells are inversely related to the pH in the calcifying fluid (Frieder et al., 2014; Zhao et al., 2018b), and incorporation of sodium into shells can be closely related to activities of ionic exchangers by which marine bivalves regulate the acid-base status at the site of calcification (Zhao et al., 2017a, 2017b). While these significant advances have been made in disentangling processes constraining the calcification sensitivity to OA, as demonstrated above, little effort has been devoted to integrating how long-term OA will affect calcification processes when considered together, thus constraining our ability to assess the extent of the calcification plasticity in response to OA.

Experiments performed across multiple generations can likely provide a means to understand the acclimation potential and mechanistic basis of marine bivalves in a rapidly acidifying ocean. A growing body of transgenerational studies, for example, demonstrates that marine bivalves (at least species hitherto studied) may have the ability to respond plastically and acclimate rapidly to OA scenarios projected by the end of this century (e.g., Ross et al., 2016; Thomsen et al., 2017; Byrne et al., 2020; Zhao et al., 2020a). However, despite the great potential of transgenerational experiments in examining whether bivalves can keep up with the pace of OA, their relatively long generation times (from months to years) and complex life cycles complicate multigenerational experiments. In addition, almost all transgenerational experiments have been carried out under simulated conditions. In the face of multiple stressors and complexities of the nature, whether rapid transgenerational acclimation can be still maintained remains unknown. Hence, approaches which can document the acclimation plasticity under environmentally realistic scenarios are in high demand.

A space-for-time approach opens a promising avenue in examining the extent to which marine bivalves have the capacity to acclimate to OA. Synchronic comparisons of individuals naturally growing along large gradients of pCO_2 and pH to substitute space for time, so-called the space-for-time substitution (Reusch, 2014), can likely capture long-term ecological relevance and more accurately assess the fate of key species, populations, and ecosystems under projected OA scenarios. Naturally CO_2-

enriched habitats, especially volcanic CO_2 seeps that can generate consistently acidic conditions throughout the year, are increasingly used as natural analogues of future ocean acidification conditions (Feely et al., 2008; Hall-Spencer et al., 2008; Rastrick et al., 2018). Within the framework of space-for-time substitution, the large predatory gastropod *Charonia lampas* living in CO_2 seeps off Shikine Island (Japan) and the widespread Mediterranean mollusc *Hexaplex trunculus* in Vulcano Island CO_2 seeps (Italy) show little ability to compensate for corrosive effects of seawater acidification on shell mineralization (Harvey et al., 2016, 2018). Nevertheless, contrasting findings have recently been observed in molluscs inhabiting CO_2 seeps in the south-western Pacific, where the herbivorous gastropod *Eatoniella mortoni* produces thicker, more crystalline, and mechanically resilient shells for compensatory growth (Leung et al., 2019). These discrepancies among CO_2 seep habitats can most likely be attributed to differences in duration, frequency, and intensity of acidification (Aiuppa et al., 2021). To the best of our knowledge, nevertheless, only a few studies have used natural CO_2 seeps to advance our knowledge of the acclimation of marine bivalves to projected OA scenarios (e.g., Hahn et al. 2012; Agostini et al. 2018; Martins et al. 2021).

Japanese volcanic CO_2 seeps, especially those off Shikine Island, have recently been developed as natural analogues of future oceanic conditions to show how marine organisms and ecosystems respond and acclimate to OA (e.g., Inoue et al., 2013; Agostini et al., 2018, 2021; Cattano et al., 2020; Harvey et al., 2018, 2020, 2021a, 2021b). The intertidal rocky shore communities along the coast of Shikine

Island are composed predominantly of calcifying species (mussels, oysters, barnacles, coralline algae, etc.), whose abundance and distribution vary in both space and time. Surveys using quadrats (25 × 25 cm) showed that the population density of intertidal mussels near the CO_2 seeps was reduced compared to outside the seeps (from 7 ± 13 individuals to 2 ± 3 individuals; Agostini et al., 2018), indicating that they may be negatively impacted by elevated pCO_2 conditions and hence sparking our interest in testing whether, and to what extent, bivalves living near Shikine Island CO_2 seeps have the ability to acclimate under these naturally acidified conditions.

Here, we aimed at gaining a better understanding of the acclimation potential of the widely distributed mussel *Septifer bilocularis* along the coast of Shikine Island to ocean acidification. Firstly, we performed a 2-month reciprocal transplant of mussels between an elevated pCO_2 area and an adjacent reference pCO_2 area to assess their physiological performance. Secondly, we performed ultra-high-resolution temporal analysis (on a subset of individuals) of shell geochemistry along growth layers to gain temporal information for their lifespan. Geochemical approaches, such as stable carbon and nitrogen isotopic and trace elemental analyses which hold great promise to disentangle calcification responses of marine bivalves to ocean acidification in temporal context (as reviewed by Zhao et al., 2020a), were employed to obtain an integrated insights into mechanisms behind mussel calcification and associated physiological processes. Our findings provide a more comprehensive understanding about how mussels respond and likely acclimate in a rapidly acidifying ocean.

2. Materials and methods

2.1. Study area

Shikine Island (34°19'9" N, 139°12'18" E) is a volcanic island located off the Izu peninsula in Japan. The shore of the island is composed of crustal rocks varying in size with the tidal range less than 2 m, and near CO_2 seeps the water depth is approximate 4 m during high tides. As schematically illustrated in Fig. 1, our two low intertidal sites, elevated pCO_2 area and reference pCO_2 area, have well characterized carbonate chemistry (e.g., Agostini et al., 2015, 2018; Cattano et al., 2020; Harvey et al., 2018, 2020, 2021a, 2021b; Witkowski et al., 2019). The carbonate chemistry of the two sites at the time of the current study are published in Harvey et al. (2020). Briefly, seawater pH_T, temperature and salinity of the two sites were recorded through *in situ* measurements of the subtidal environment using a multisensor (WQC-24, TOA-DKK, Japan). Total alkalinity samples were collected as discrete samples and measured by titration (916 Ti-Touch, Metrohm) with 0.1 mol l^{-1} HCl. Seawater carbonate system parameters were calculated from temperature, salinity, pH_T and total alkalinity using the software CO2SYS (Pierrot et al., 2006). The reference pCO_2 area had a mean pH_T of 8.041 ± 0.067 (SD) and the elevated pCO_2 area had a mean pH_T of 7.719 ± 0.095 (SD). The elevated pCO_2 area represents an end of the present century projection for reductions in pH under the Representative Concentration Pathway 8.5 scenario (IPCC, 2013), and had the same temperature, salinity, dissolved oxygen, total alkalinity, nutrients and depth as the reference site

(Agostini et al., 2015, 2018; Harvey et al., 2019, 2021a), as well as the same carbon isotopic ratio of dissolved inorganic carbon (Fig. 1) relative to the reference pCO_2 area used for comparison. The gas emitted from the seeps is 98% CO_2 (Agostini et al., 2015). The annual range of sea surface temperature varies from 14 to 28 °C and salinity remains constant at ca. 34 over time (Agostini et al., 2018; Harvey et al. 2021a).

2.2. Study organism

Mytilidae represent some of the most conspicuous marine bivalves within the intertidal and shallow subtidal zones (Morton, 2019). Species of *Septifer* (Récluz, 1848), along with many warm-water Mytilidae, are far less well studied when compared to genera such as *Mytilus* and *Perna* (Morton et al. 2020). *Septifer bilocularis* (Linnaeus, 1758), our study organism, is located along the coasts of mainland Japan, as well as in the Indo-West-Pacific (Higo et al. 1999). Individuals of *S. bilocularis* have a thick, ovally elongate shell that is ventrally concave, dorsally peaked with a rounded posterior margin with terminal beaks (Morton et al. 2020). The shell valves are covered by a thick periostracum over fine radially divaricating lirae (Morton et al. 2020). This species was the dominant mussel within our study site, and yet little else about its ecology has previously been described. Individuals of *S. bilocularis* in Hong Kong are subtidal and associated with coral heads (Dudgeon and Morton, 1982), whereas individuals (shell length of 23–28 mm and body weight of 2.3–2.5 g) in our study site are found attached by byssal threads to the rocky

196 substratum in the low intertidal zone.

197

198 ***2.3. Experimental setup***

199 Adults of *S. bilocularis* inhabiting the low intertidal zone in the elevated pCO_2 and
200 reference pCO_2 areas were randomly collected, individually labelled with a reference
201 number using queen bee marking tags (E.H. Thorne Ltd., UK), and reciprocally
202 transplanted for two months (mid-April to mid-June 2019) using a two-way
203 orthogonal experimental design (as schematically illustrated in Fig. 1). This design
204 therefore includes procedural controls where some individuals were transplanted
205 back into the same site they were collected from. Redeployment of individuals for
206 the two-month reciprocal transplantation was achieved by placing them inside cages
207 (green mesh, 20 × 10 × 4 cm, 1 cm mesh size) which were attached to the substratum
208 with anchor bolts in locations next to where the mussel individuals were originally
209 collected in the low intertidal zone (two cages per site) at the same tidal height (with
210 a maximum tidal depth of around 2.0 m during spring tides). Each cage contained
211 five individuals collected from reference pCO_2 conditions and five individuals
212 collected from elevated pCO_2 conditions (individuals were randomly assigned to the
213 four cages). Seawater samples for the stable carbon isotope ratio ($\delta^{13}C$) analysis were
214 collected using 20-ml glass vials and poisoned with two drops of the supersaturated
215 mercury chloride solution to prevent any biological interference.

216

217 Following the *in situ* transplant experiment, two individuals from each site

(elevated pCO_2 and reference pCO_2) were used for high-resolution analysis over their lifespan to identify ontogenetic age, annual growth rate, and geochemical properties via stable isotopic analysis (described in greater detail below). These individuals were selected from the reciprocal transplant experiment, at random (one from each cage), using only those procedural control individuals that had been collected from, and transplanted back into the same site.

2.4. Sample collection and individual analysis

Following our *in situ* transplant experiment, all specimens were carefully cleaned and then frozen at –20 °C. Four or five individuals from each of the four treatments of the reciprocal transplant were randomly sampled and dissected using a scalpel for analysis. The whole soft tissue of each mussel was washed with Milli-Q water (18.2 mΩ), freeze-dried for 48 h and then weighed, and the shell air-dried and weighed. The condition index (CI) of each sample was calculated using the equation (1) (Lucas and Beninger, 1985).

$$CI = dtw/dsw \times 100 \quad \text{.....(1)}$$

where CI is the condition index, and dtw and dsw represent the dry soft tissue weight (g) and dry shell weight (g), respectively.

The newly formed shell portion of each mussel was analyzed to examine its daily

240 growth rate. Specifically, mussel shells were sectioned to accurately analyze the rate
241 of shell growth and thickness of periostracum formation during the experiment. The
242 right valve of each shell was embedded in epoxy resin and along the axis of
243 maximum growth two three-millimeter-thick sections were cut using a low-speed
244 diamond saw (Isomet 1000, Buehler, Lake Bluff, IL, United States). Afterward, both
245 sections were mounted on glass slides, ground with 70 and 13 µm diamond cup
246 whetstones, respectively, polished with 0.3 µm alumina powder, and then
247 ultrasonically washed with Milli-Q water (18.2 mΩ) to remove any adhering particles.
248 Photographs of polished shell sections were taken using a digital microscope
249 (KEYENCE VHX-2000) and the amount of newly formed shell portions (as determined
250 by internal growth bands; Zhao et al., 2019a) and also thickness of corresponding
251 periostracum were analyzed using an image processing software ImageJ. The average
252 daily rate of mussel shell growth during the experiment was subsequently computed.
253
254 To perform high-resolution analysis across the lifespan of the mussel, the
255 mussels subsampled from the reciprocal transplant experiment were used (one
256 mussel from each cage in the elevated pCO_2 area, and one mussel from each cage in
257 the reference pCO_2 area). We only used individuals collected from and transplanted
258 back into the same site. These mussels were soaked in 0.5 wt% HCl overnight at room
259 temperature to prevent shell surface contamination (Zhao et al., 2019b). Carbonate
260 samples from the left valve of each mussel were then milled along the axis of
261 maximum shell growth at approximately 0.1-0.3 mm resolution for subsequent

geochemical analysis.

2.5. Isotopic analysis via EA-IRMS and CF-IRMS

Approximately 2 mg of soft tissue from each mussel was homogenized and weighed into a tin capsule, tightly folded, and then analyzed using an elemental analyzer (EA; vario MICRO cube, Elementar, Germany) interfaced to an isotope ratio mass spectrometer (IRMS; IsoPrime100, IsoPrime, UK) at the Atmosphere and Ocean Research Institute (AORI), University of Tokyo. Stable carbon and nitrogen isotope ratios ($\delta^{13}C$ and $\delta^{15}N$) were reported related to the standards (Vienna Pee Dee Belemnite (VPDB) and the atmospheric nitrogen, respectively), and expressed in the conventional delta (δ) notation in per mil (‰). Measured $\delta^{13}C$, $\delta^{15}N$ and C/N ratio were calibrated respectively against standards (L-alanine (AZ101SS13), Shoko Scientific; $\delta^{13}C$ = –19.6 ‰, $\delta^{15}N$ = 13.7, and C/N = 3.0). Throughout the analysis, the NIST SRM 2976 (National Institute of Standards and Technology, United States) was used to monitor instrumental conditions. The reproducibility was better than 0.28 ‰ for $\delta^{13}C$ (1 δ) and 0.10 ‰ for $\delta^{15}N$ (1 δ).

To measure stable carbon and oxygen isotope ratios ($\delta^{13}C$ and $\delta^{18}O$) of the shell, approximately 100 µg of carbonate powder milled from the newly formed shell portion was weighed into a glass vial and then reacted with 100 % phosphoric acid at 72 °C in a helium-flushed borosilicate exetainer for one hour. Liberated CO_2 gas was analyzed using a Thermo Finnigan Delta V Plus continuous flow-isotope ratio mass

spectrometer (CF-IRMS) coupled to a Thermo Finnigan GasBench II at AORI. Measured $\delta^{13}C$ and $\delta^{18}O$ data were calibrated against NBS-19 ($\delta^{13}C$ = +1.95 ‰; $\delta^{18}O$ = –2.20 ‰). Shell $\delta^{13}C$ and $\delta^{18}O$ values were calculated against VPDB, reported in δ-notation and then given as ‰. Profiles of $\delta^{18}O_{shell}$ provide a chronological framework, with each shell portion placed into a temporal context allowing the ontogenetic age of each specimen to be determined. By doing so, the implications of ontogeny in the interpretation of results from reciprocal transplantation can be substantially eliminated. The reproducibility was better than 0.05 ‰ for $\delta^{13}C$ (1 δ) and 0.23 ‰ for $\delta^{18}O$ (1 δ). Seawater $\delta^{13}C$ analysis was performed using CF-IRMS, calibrated and calculated in the same manner as shell $\delta^{13}C$ values.

2.6. Elemental analysis via LA-ICP-MS

Concentrations of boron (B), Sodium (Na), Magnesium (Mg), Phosphorus (P), Potassium (K), Strontium (Sr), Barium (Ba), and Uranium (U) in polished shell sections were analyzed by laser ablation inductively coupled plasma mass spectrometry (LA-ICP-MS) in 'spot' mode at AORI. Three to six discrete spots based on the incremental length in the newly formed shell portion during the experiment were set in each shell. Analyses were performed with an excimer-based laser ablation system (NWR-193, New Wave Research, Fremont, CA, United States) connected to ICP-MS (7700 CS, Agilent, Tokyo, Japan). The laser was operated at a pulse rate of 10 Hz, pulse energy of 1.8 mJ, and beam diameter of 100 µm. Helium was used as the carrier gas. Prior to each ablation backgrounds were analyzed for 7 s, and subsequent ablation time was

15 s followed by 25 s wash out. The signal intensity of ions (^{10}B, ^{23}Na, ^{24}Mg, ^{31}P, ^{39}K, ^{43}Ca, ^{88}Sr, ^{138}Ba, ^{238}U) was calculated by subtracting the background level of trace elements empirically obtained with the 0 % laser output set. ^{43}Ca was used as internal standard and the element-to-^{43}Ca ratio was computed and compared to the standard reference material signal intensity. NIST SRM 612 (synthetic glass) was used as an external standard, and giant clam powder JCt-1 and coral powder JCp-1 (National Institute of Advanced Industrial Science and Technology, Tsukuba, Japan) were measured as quality control materials to confirm accuracy. Calculations on trace element-to-calcium ratio were based on analyses of NIST SRM 612. To monitor the instrumental drift, all reference materials were analyzed after every 10-20 samples.

2.7. Statistical analysis

The $\delta^{13}C$ composition of bivalve shells is controlled by seawater $\delta^{13}C_{DIC}$, the $\delta^{13}C$ of metabolically generated CO_2, as well as the proportion of metabolic CO_2 incorporated into shell carbonate (McConnaughey and Gillikin, 2008). Hence, determination of the relative contribution of metabolic carbon can be achieved according to the following equation (2) described by McConnaughey et al. (1997).

$$\%C_M = (\delta^{13}C_{shell} - \varepsilon_{cal\text{-}b} - \delta^{13}C_{DIC})/(\delta^{13}C_M - \delta^{13}C_{DIC}) \times 100 \quad (2)$$

where $\%C_M$ is the percentage of metabolic carbon incorporated into shell carbonate. $\delta^{13}C_{shell}$, $\delta^{13}C_{DIC}$ and $\delta^{13}C_M$ represent the $\delta^{13}C$ of shell carbonate, seawater dissolved

328 inorganic carbon (DIC) and metabolic carbon, respectively, and $\varepsilon_{cal\text{-}b}$ represents the
329 enrichment factor between calcite and bicarbonate (1 ‰ calculated by Romanek et
330 al., 1992). In the present study, the $\delta^{13}C$ ratios of mussel soft tissues were employed
331 to approximate $\delta^{13}C_M$ according to McConnaughey et al. (1997).
332
333 All data generated following reciprocal transplantation were analyzed using the
334 IBM SPSS Statistics version 19.0 (SPSS Inc., Chicago, IL, USA). Shapiro-Wilk's test and
335 Levene's F-test were performed to examine the normal distribution (normality) and
336 equal variance among groups (homoscedasticity) of experimental data. A fixed-
337 effects analysis of variance (ANOVA) model of pCO_2 (2 levels, reference pCO_2 and
338 elevated pCO_2) and origin (2 levels, reference pCO_2 and elevated pCO_2) was used for
339 the analysis. Following the two-way ANOVA, a Fisher's Least Significant Difference
340 (LSD) post-hoc test was performed to test the significance of experimental data
341 among groups designated according to the two-way orthogonal experimental design.
342 Statistical significance was set at $p < 0.05$. The fixed-effects model was initially
343 compared to a mixed-effects model using the 'transplant cage' as a random-effect for
344 each endpoint measurement. In all cases, the fixed effects model did not significantly
345 differ from the mixed effects model and demonstrated lower AIC scores. As such, the
346 more parsimonious fixed-effects model was employed.
347

348 # 3. Results

349 ## 3.1. Growth performance following transplantation

No mortality was recorded over the course of the transplant experiment. No statistically significant differences in physiological traits were observed for mussels transplanted within the same areas (i.e., elevated pCO_2 or reference pCO_2 conditions), irrespective of their origin under elevated or reference pCO_2 conditions ($p > 0.05$; Figs. 2a and 2b). Residing in elevated pCO_2 conditions significantly affected the physiological performance of the mussels, as best exemplified by significant decreases in their condition index ($p < 0.05$; Fig. 2a) and shell growth ($p < 0.05$; Fig. 2b). Nevertheless, neither pCO_2 conditions nor the reciprocal transplantation, and their interaction, significantly affected the thickness of mussel shell periostracum ($p > 0.05$; Fig. 2c).

3.2. Somatic stable isotopic signatures following transplantation

Mussels collected under reference pCO_2 conditions showed significantly higher $\delta^{13}C_{soft\ tissue}$ values than those inhabiting elevated pCO_2 conditions ($p < 0.05$; Fig. 3a). Mussel $\delta^{15}N_{soft\ tissue}$ signatures were only significantly affected by reciprocal transplantation, with values significantly higher in mussels collected from reference pCO_2 areas than those typically residing in elevated pCO_2 areas when experimentally exposed to elevated pCO_2 ($p < 0.05$; Fig. 3b). Mussel C/N ratios were not significantly affected by either pCO_2 conditions or reciprocal transplantation ($p > 0.05$; Fig. 3c).

3.3. Shell geochemical properties following transplantation

While the shells of mussels collected from reference pCO_2 areas had consistently

lower $\delta^{13}C_{shell}$ values in comparison with those in elevated pCO_2 areas (Fig. 4a), no significant effect of reciprocal transplantation was found ($p > 0.05$). $\delta^{13}C_{shell}$ ratios were also not significantly affected by pCO_2 conditions ($p > 0.05$). Interaction between these two factors exhibited significant effects on $\delta^{18}O_{shell}$ ratios ($p < 0.05$; Fig. 4b). Under acidified conditions, mussels collected from reference pCO_2 areas showed significantly lower $\delta^{18}O_{shell}$ values than those previously inhabiting elevated pCO_2 areas ($p < 0.05$). Furthermore, as shown in Fig. 4c, seawater DIC was determined as the predominant source of shell carbonate, and its contribution to the DIC pool at the site of calcification increased with increasing pCO_2 concentration.

Element-to-calcium ratios of mussel shells following transplantation are shown in Fig. 5. With increasing pCO_2 concentration, the amount of B (Fig. 5a) and U (Fig. 5h) incorporated into shell carbonate decreased significantly ($p < 0.05$). Nevertheless, the incorporations of Na (Fig. 5b), Mg (Fig. 5c), P (Fig. 5d), K (Fig. 5e), Sr (Fig. 5f), and Ba (Fig. 5g) were not significantly affected by either pCO_2 conditions or the reciprocal transplantation ($p < 0.05$).

3.4. Analysis of shell geochemical properties over the lifespan

As illustrated in Fig. 6a, high-resolution $\delta^{18}O_{shell}$ profiles of mussels originally living under reference pCO_2 conditions and under elevated pCO_2 conditions were extracted to constrain the ontogenetic age and rates of annual shell growth. Two mussels randomly selected from the reference pCO_2 areas were 7-years-old and 5-years-old,

394 and those living in the elevated pCO_2 areas were 7-years-old and 6-years-old,
395 respectively. Following placing each shell portion into a precise context, it is evident
396 that across their entire lifespan mussels inhabiting elevated pCO_2 conditions grew at
397 slower rates in comparison with those living under reference pCO_2 conditions (Fig.
398 6b). $\delta^{13}C_{shell}$ profiles provide consistent evidence of lower $\delta^{13}C_{shell}$ values in mussels
399 living under reference pCO_2 conditions than those under elevated pCO_2 conditions
400 (Fig. 6c).
401

402 ## 4. Discussion

403 This is the first investigation of calcification responses of marine bivalves living
404 around Japanese volcanic CO_2 seeps. Our observations of significantly lowered shell
405 growth with increasing elevated pCO_2 indicate that mussels inhabiting elevated pCO_2
406 conditions have their shell formation negatively impacted and do not appear to be
407 capable of rapidly acclimating to ocean acidification scenarios projected by the end
408 of this century. These observations are in line with findings of drastically decreased
409 abundance of bivalves with increasing levels of pCO_2 along the shore of Shikine Island
410 (Agostini et al., 2018; Hall-Spencer et al., 2022). Similar observations have also been
411 made at CO_2 seeps off islands of São Miguel and Faial in the North Atlantic Ocean,
412 where the abundance, size and net-calcification of the bivalve (*Ervilia castanea*) were
413 inversely related to pCO_2 levels (Martins et al., 2021). Yet, it is worth noting here that
414 the declines in shell formation under elevated pCO_2 conditions at CO_2 seeps are at
415 odds with previous conclusions that demonstrated marine bivalves inhabiting

naturally CO_2-enriched habitats, such as upwelling areas, can maintain the ability to calcify by implementing compensatory mechanisms to mitigate effects of elevated pCO_2 on shell calcification (e.g., Thomsen et al., 2017; Zhao et al., 2018b). In addition, a growing body of transgenerational experiments has shown that a suite of physiological processes underpinning the shell calcification can respond plastically and acclimate rapidly to near-future OA scenarios (e.g., Fitzer et al., 2014; Parker et al., 2015; Zhao et al., 2017b, 2018a). Given that volcanic CO_2 seeps can be more reliably used as natural analogues of future oceanic conditions than many other naturally CO_2-enriched systems (Rastrick et al., 2018), discrepancies among studies deserve further attention. Hence, the elucidation of the underlying mechanisms would represent a key leap forward in our understanding of how bivalves will respond and acclimate in a rapidly acidifying ocean.

4.1. Changes in dietary regimes of mussels under elevated pCO_2 conditions

Following reciprocal transplantation, the condition index of the mussels, which is widely used as an indication of the energy budget of bivalves (Lucas and Beninger, 1985), significantly decreased for those individuals held under the elevated pCO_2 conditions, indicating decreases in their energy reserves. Reduced energy reserves in mussels under acidified conditions can partly be explained by changes in their dietary regimes. For the first time, the present study utilized $\delta^{13}C$ and $\delta^{15}N$ ratios of mussel soft tissues as dietary tracers and revealed marked shifts in food sources of mussels living in reference and elevated pCO_2 areas. Significant changes in mussel $\delta^{13}C_{soft\ tissue}$

438 and $\delta^{15}N_{soft\ tissue}$ demonstrate changes in their principal food sources, which largely
439 stem from algal detritus (Zhao et al., 2013). Evidence in support of this interpretation
440 further comes from recent surveys around the same set of CO_2 seeps off Shikine
441 Island by Harvey et al. (2021a), according to which diatom algal turfs (*Biddulphia*
442 *biddulphiana*) largely replaced seaweeds and became the dominant habitat-forming
443 species around the CO_2 seeps, thereby potentially affecting components of organic
444 detritus. Given significant decreases in condition index and thereby energy reserves,
445 these shifts in food sources are likely much less beneficial for mussel calcification in
446 response to long-term elevated pCO_2 stress.
447
448 Nevertheless, it is worth noting here that only the combination of both quality
449 and quantity of food could reliably dictate dietary regimes of mussels at CO_2 seeps.
450 Without doubt, in the present study food sources of mussels varied as pCO_2 levels
451 rose, but it remains largely unknown how the nutritional quality of food (which can
452 be expressed in terms of C:N ratios) responded. At a CO_2 shallow vent system off
453 Ischia in the Mediterranean Sea, lowered C:N ratios of organic matter sources with
454 increasing pCO_2 levels can likely indicate higher nutritional quality of food produced
455 by primary producers (Ricevuto et al., 2015). Also, the dominant calorie-enriched turf
456 algae near CO_2 seeps in New Zealand had lower C:N ratio (and thus higher nutritional
457 quality) than that of seaweeds outside seeps (Leung et al., 2018, 2020). Presumably,
458 in the present study mussels might even consume higher nutritional quality of food
459 sources under acidified conditions, but evidently such an increase in the quality of

food could still be insufficient for compensating against calcification declines.

Feeding is fundamental for marine bivalves to acquire energy, and its plasticity is therefore a prerequisite for acclimation in a rapidly acidifying ocean. As reviewed by Clements and Darrow (2018), many bivalve species experienced depressed feeding rates and thus reduced energy acquisition when exposed to elevated pCO_2. Yet, little information is available about the role played by the food availability, mainly because most laboratory-based experiments are carried out under the same feeding regimes. In the field, previous studies within upwelling systems have demonstrated that food availability could be sufficient for mussels to maintain shell growth and tissue energy reserves, while still fulfilling increased energy demands under acidified conditions (e.g., Parker et al., 2015; Zhao et al., 2018b, 2019a; Ramajo et al., 2020). At CO_2 seeps off Shikine Island, while ocean acidification resulted in marked shifts in ecosystems dominated by turf algae (Harvey et al., 2021a), due to the CO_2 fertilization, turf algae can be more likely to rapidly proliferate than macroalgae outside seeps (Harvey et al., 2021b). The availability of food stemming from predominant turf algal detritus for mussels living around CO_2 seeps might be particularly abundant. The role played by turf algae in the quality and availability of food for mussel consumption deserves further investigation.

Taken together, considering significant decreases in condition index and shell growth, it is reasonable to assume that evident shifts in dietary regimes which may

be beneficial for energy acquisition are not sufficient to fully compensate for the impact of OA on mussel shell formation. As demonstrated below, it is likely that a re-partitioning of energy amongst different shell calcification processes may occur.

4.2. Mechanisms of mussel calcification at CO_2 seeps are less energetically efficient

Understanding the sensitivity of calcification to OA requires an appreciation of the regulation of calcifying fluid carbonate chemistry. Identification of sources and pathways of dissolved inorganic carbon (DIC) at the calcifying front has greatly improved our knowledge in this regard. Up to 100% of shell carbonate was composed of seawater DIC suggesting that mussels almost exclusively extract external seawater DIC rather than internal metabolic CO_2 to calcify. While this finding agrees well with the theoretical calculation of the respiratory gas exchange model, whereby seawater DIC contributes more than 90% of the calcifying fluid DIC pool (McConnaughey et al., 1997), evidence is accumulating that marine bivalves, especially under OA stress, can preferentially transport metabolic CO_2 as a more efficient and less costly compensatory mechanism to regulate the carbonate chemistry of their calcifying fluid (e.g., Gillikin et al., 2007; Zhao et al., 2018a; Lu et al., 2019; Lee et al., 2021). Up to 61% of metabolic carbon, for example, was observed in shells of Manila clams (*Ruditapes philippinarum*) which exhibited rapid acclimation to high pCO_2 following transgenerational exposure (Zhao et al., 2018a). Considering that cellular membranes are highly CO_2 permeable (Gutknecht et al., 1977), metabolic CO_2 can passively diffuse into the calcifying fluid, where it is quickly

transformed to HCO_3^- through the hydration of carbonic anhydrase (Zhao et al., 2020b). In comparison to the passive diffusion of metabolic CO_2, the transport of seawater DIC for calcification is thought to be energetically expensive, since the active transport of HCO_3^- (the most likely calcification-relevant DIC species in seawater) from the ambient seawater to the calcifying front requires many ion channels, exchangers, and transporters (as reviewed in Zhao et al., 2020a). The reason that mussels inhabiting the elevated pCO_2 conditions have mainly employed mechanisms for active transport of seawater DIC rather than less costly preferential uptake of metabolic CO_2 as calcifying substrates remains unknown, but it is intriguing that the latter usually is seen in bivalves inhabiting intertidal zones where they habitually experience aerial exposure during the low tide and therefore are used to counter respiratory acidosis caused by the retention of metabolic CO_2 (Booth et al., 1984; Burnett, 1988). Since the mussels used here were located in the very low intertidal, it is possible that metabolic CO_2 production during the relatively short aerial exposure is insufficient to maintain calcification rates, necessitating the use of the more energetically-costly seawater-derived HCO_3.

Active removal of protons generated during the $CaCO_3$ precipitation at the site of calcification is a fundamental requirement for stress tolerance and acclimation to OA. With increasing pCO_2 concentrations, the amounts of pH-sensitive elements such as B and U incorporated into mussel shells decreased significantly, demonstrating declines of pH at the site of calcification. Similar results have been documented in a

526 variety of coastal bivalves acutely exposed to OA scenarios projected by the end of
527 this century (e.g., Heinemann et al., 2012; Frieder et al., 2014; Liu et al., 2015; Zhao
528 et al., 2018b). Perhaps most notably, virtually unaffected Na/Ca_{shell} and K/Ca_{shell} ratios
529 demonstrate that mussels may be unable to complement a suite of less costly and
530 more efficient ion-regulatory machineries equipped in the mantle tissue, especially
531 Na^+/H^+ exchanger (Zhao et al., 2017a; Ramesh et al., 2018), for the removal of
532 excessive protons in the calcifying fluid. If this is the case, then one would expect
533 that energy-requiring H^+-ATPase may play a major role in actively pumping protons
534 out of the site of calcification. Taken together, it is reasonable to assume that mussels
535 collected within the elevated pCO_2 areas do not possess compensatory mechanisms
536 that are energetically efficient in the maintenance of calcifying fluid acid-base
537 homeostasis under OA stress.
538
539 Considering the corrosive nature of acidified waters within the elevated pCO_2
540 areas, it is also imperative to account for the degree to which shell calcification could
541 be counteracted by dissolution and erosion. It has been documented that gastropods,
542 *Charonia lampas*, collected at our study sites exhibited serious shell dissolution and
543 visible deterioration (Harvey et al., 2018), due to loss of periostracum – an external
544 organic cover protecting shells from corrosive seawater (Saleuddin and Petit, 1983).
545 When maintained under elevated pCO_2 conditions for two months, mussels did not
546 lose the thickness of periostracum in the newly formed shell portion and undergo
547 progressive shell dissolution and erosion, indicating that their shell properties may

548 not be as susceptible to seawater acidification as *C. lampas*. Hence, the resilience of
549 marine bivalves to calcify in an acidifying ocean also depends on their ability to
550 counter periostracum loss and shell dissolution. The $\delta^{13}C$ analysis indicates that the
551 formation of mussel periostracum is mediated by organic matrix synthesized and
552 secreted from the outer mantle epithelium (Zhao et al., 2019b), the latter known to
553 be extremely energetically expensive and equivalent to 60% of the energy demands
554 of somatic growth or 150% of the energetic demands of gamete development
555 (Palmer, 1992). The maintenance of periostracum formation thus indicate that under
556 acidified conditions mussels give priority to the shell defence rather than calcification,
557 especially considering that accumulating evidence suggests that the total amount of
558 energy allocated for shell formation declines considerably under acidified conditions,
559 (Waldbusser et al., 2013; Li et al., 2016; Spalding et al., 2017; Leung et al., 2020b).
560 Compensatory mechanisms such as the production of alternative calcium carbonate
561 polymorphs (e.g. Leung et al. 2017) or the production of thicker shells (e.g. Cross et
562 al. 2019) may additionally help to counteract the negative effects of ocean
563 acidification on the shell morphology. By combining findings obtained from reciprocal
564 transplantation (i.e., the limited energy budget, the more energetically costly
565 calcification processes, and the importance of the periostracum in impeding shell
566 dissolution), it is, therefore, reasonable to assume that mussels may be forced to
567 employ functional trade-offs in their energy expenditure in order to survive under
568 elevated pCO_2 conditions.
569

570 **4.3. Mussels shrink to survive under elevated pCO_2 conditions**

571 While most calcifiers (oysters, decapods, gastropods, barnacles, etc.) had significant
572 decreases in abundance around the volcanic CO_2 seeps off Shikine Island (Agostini et
573 al., 2018), patchily distributed dense clusters of mussels were seen along the
574 gradients of CO_2, sparking interest in understanding why mussels can survive OA.
575 Limited energy budget, less energy-efficient calcification, and sustained periostracum
576 integrity are traits being exhibited by the mussels following their exposure to
577 elevated pCO_2 conditions (Thomsen et al., 2017; Zhao et al., 2017a), which however
578 cannot satisfactorily explain why mussels can survive at CO_2 seeps. High-resolution
579 analysis of shell geochemistry also indicates that mussel calcification is adversely
580 affected by high pCO_2. Evidence in support of this assumption comes from the
581 consistently higher values of $\delta^{13}C_{shell}$ profiles than those observed in control mussels,
582 indicating that mussels living near CO_2 seeps incorporate higher amount of seawater
583 inorganic carbon (which had higher $\delta^{13}C$ values than that of metabolic carbon) to the
584 site of calcification than those grown outside seeps. Hence, mussels collected from
585 the elevated pCO_2 areas adopted energetically costly strategies (e.g., active transport
586 of seawater DIC rather than the passive diffusion of metabolic carbon) to calcify. The
587 integrity of periostracum also suggests that energy is being allocated for its
588 maintenance, as demonstrated above. In line with findings following reciprocal
589 transplantation, therefore, it is reasonable to assume that mussels suffer a reduced
590 energy budget in acidified conditions.

591

592 Surprisingly, our chronological findings indicate that, despite their small size
593 (shell length 1.86 to 2.83 cm), mussels randomly chosen for reciprocal
594 transplantation were up to 7-years-old. Mussels collected near the CO_2 seeps were
595 not only older, but also grew slower than those living outside the CO_2 seeps, leading
596 to the shell length of mussels being smaller by as much as 20%. Presumably, slow
597 shell building is a strategy used by mussels to survive elevated pCO_2 conditions. A
598 similar observation has been made for two gastropod species at natural CO_2 seeps
599 off Vulcano Island, Italy, whereby the ability to adapt through dwarfing conferred a
600 physiological advantage for the smaller individuals to survive under increased CO_2
601 levels (Garilli et al. 2015).
602
603 Slow shell building can substantially lessen the energy burden of stressed
604 mussels. Similar conclusions have been often drawn on the early life stages of
605 brooding marine bivalves (e.g., Noisette et al., 2014; Lucey et al., 2015; Waldbusser
606 et al., 2016). The rates of calcification and energy consumption in the larvae of
607 brooding oysters *Ostrea lurida* for example are nearly 10 and 50 times slower than
608 those of broadcast spawning oysters *Crassostrea gigas* (Waldbusser et al., 2016).
609 Mechanisms underpinning slow shell building as a possible trait for resistance to OA
610 are suggestively associated with the kinetic-energetic constraint on shell calcification
611 (Waldbusser et al., 2013, 2014). Reductions in body length to decrease energy needs
612 when under harsh conditions has been observed in many organisms (Wikelski and
613 Thom, 2000; Sheridan and Bickford, 2011; Garilli et al. 2015). Smaller body size can

614 be an advantage as pCO_2 levels continue to rise.

615

616 The use of CO_2 seeps in this study allowed us to investigate the consequences of
617 future ocean acidification on mussel shell formation. It should be acknowledged,
618 however, that this is in the absence of concurrent ocean warming (Hughes et al.
619 2017), and changes in temperature will mediate the response of organisms and
620 communities to future ocean acidification. It may be possible in future studies, for
621 example, to carry out studies that manipulate temperature along CO_2 gradients (e.g.,
622 Alessi et al., 2019). Regardless, CO_2 seeps and other natural analogues are still
623 invaluable for assessing the future state of organisms, communities, and ecosystems
624 to future ocean acidification (Rastrick et al., 2018).

625

626 ## 5. Conclusions

627 This study is the first to provide a comprehensive understanding of how mussels
628 calcify and grow at CO_2 seeps off Shikine Island. We observed that mussels inhabiting
629 elevated pCO_2 conditions exhibited marked shifts in their food sources, and displayed
630 significant decreases in their condition index and hence tissue energy reserves. While
631 the mussels were able to survive, their shell formation was negatively impacted by
632 ocean acidification, leading to reduced growth and size. They survived through slow
633 shell building, demonstrated by high-resolution analysis of shell geochemistry over
634 their lifespan. This slow shell growth is a plastic response that allows them to
635 maintain a smaller body size, a physiological advantage to enhance energy efficiency.

These findings reveal future trajectories for marine bivalves in an acidifying ocean and provide insights into their scope for acclimation.

Acknowledgments

We thank the technical staff at Shimoda Marine Research Center, University of Tsukuba for their assistance aboard RV Tsukuba II and at the study site, and the Japan Fisheries agencies of Nijima/Shikine Island (Tokyo prefecture) for their support. This project was supported by the 'International Education and Research Laboratory Program', University of Tsukuba, and contributes towards the International CO_2 Natural Analogues (ICONA) Network. This work was also supported by JSPS KAKENHI Grant Number 17K17622 and 17P17333, and we also acknowledge funding support from the Ministry of Environment, Government of Japan (Suishinhi: 4RF-1701), the National Natural Science Foundation of China (42076121, M-0163, 42211530423), the Guangdong Zhujiang Talents Program (2021QN02H665), the Department of Education of Guangdong Province (2020KTSCX050, 2022ZDZX4012) and the program for Scientific Research Start-up Funds of Guangdong Ocean University.

Data Availability Statement

The data that support the findings of this study are openly available in PANGAEA.

References

Agostini, S., Harvey, B.P., Wada, S., Kon, K., Milazzo, M., Inaba, K., Hall-Spencer, J.M.,

2018. Ocean acidification drives community shifts towards simplified non-calcified habitats in a subtropical-temperate transition zone. Sci. Rep. 8, 111354.

Agostini, S., Houlbrèque, F., Biscéré, T., Harvey, B. P., Heitzman, J. M., Takimoto, R., Yamazaki, W., Milazzo, M., Rodolfo-Metalpa, R., 2021. Greater mitochondrial energy production provides resistance to ocean acidification in "winning" hermatypic corals. Front. Mar. Sci. *7*, 1235.

Agostini, S., Wada, S., Kon, K., Omori, A., Kohtsuka, H., Fujimura, H., Tsuchiya, Y., Sato, T., Shinagawa, H., Yamada, Y., Inaba, K., 2015. Geochemistry of two shallow CO_2 seeps in Shikine Island (Japan) and their potential for ocean acidification research. Reg. Stud. Mar. Sci. 2, 45-53.

Aiuppa, A., Hall-Spencer, J. M., Milazzo, M., Turco, G., Caliro, S., Di Napoli, R., 2021. Volcanic CO_2 seep geochemistry and use in understanding ocean acidification. Biogeochemistry 152, 93-115

Alessi, C., Giomi, F., Furnari, F., Sarà, G., Chemello, R., Milazzo, M., 2019. Ocean acidification and elevated temperature negatively affect recruitment, oxygen consumption and calcification of the reef-building *Dendropoma cristatum* early life stages: Evidence from a manipulative field study. Science of The Total Environment, 693, 133476.

Blunden, J., Derek, S.A., Hartfield, G., 2018. State of the climate in 2017. Bull. Am. Meteorol. Soc. 99.

Booth, C.E., McDonald, D.G., Walsh, P.J., 1984. Acid-base balance in the sea mussel, *Mytilus edulis*. II: effects of hypoxia and air-exposure on hemolymph acid-base

680 status. Mar. Biol. Lett. 5, 359-369.
681 Burnett, L.E., 1988. Physiological responses to air exposure: acid-base balance and
682 the role of branchial water stores. Am. Zool. 28, 125-135.
683 Byrne, M., Foo, S.A., Ross, P.M., Putnam, H.M., 2020. Limitations of cross- and
684 multigenerational plasticity for marine invertebrates faced with global climate
685 change. Global Change Biol. 26, 80-102.
686 Caldeira, K., Wickett, M.E., 2003. Oceanography: anthropogenic carbon and ocean pH.
687 Nature 425, 365.
688 Clements, J.C., Darrow, E.S., 2018. Eating in an acidifying ocean: a quantitative review
689 of elevated CO_2 effects on the feeding rates of calcifying marine invertebrates.
690 Hydrobiologia 820, 1-21.
691 Cross, E.L., Harper, E.M., Peck, L.S., 2019. Thicker shells compensate extensive
692 dissolution in brachiopods under future ocean acidification. Environmental
693 Science & Technology, 53(9), 5016–5026.
694 Dudgeon D., Morton B., 1982. Coral associated Mollusca of Tolo Harbour, Hong Kong.
695 Morton B., Tseng C.K. (Eds.), Proceedings of the First International Marine
696 Biological Workshop: The Marine Flora and Fauna of Hong Kong and southern
697 China, Hong Kong, Hong Kong University Press, Hong Kong, pp. 627-650.
698 Ekstrom, J.A., Suatoni, L., Cooley, S.R., Pendleton, L.H., Waldbusser, G.G., Cinner, J.E.,
699 Ritter, J., Langdon, C., Hooidonk, R.V., Gledhill, D., Wellman, K., Beck, M.W.,
700 Brander, L.M., Rittschof, D., Doherty, C., Edwards, P., Portela, R., 2015.
701 Vulnerability and adaptation of US shellfisheries to ocean acidification. Nat. Clim.

Change 3, 207-214.

Feely, R.A., Sabine, C.L., Hernandez-Ayon, J.M., Ianson, D., Hales, B., 2008. Evidence for up-welling of corrosive “acidified” water onto the continental shelf. Science 320, 1490-1492.

Fitzer, S.C., Caldwell, G.S., Phoenix, V.R., Kamenos, N.A., 2014. Ocean acidification reduces the crystallographic control in juvenile mussel shells. J. Struct. Biol. 188, 39-45.

Frieder, C.A., Gonzalez, J.P., Levin, L.A., 2014. Uranium in larval shells as a barometer of molluscan ocean acidification exposure. Environ. Sci. Technol. 48, 6401-6408.

Garilli, V., Rodolfo-Metalpa, R., Scuderi, D., Brusca, L., Parrinello, D., Rastrick, S.P.S., Foggo, A., Twitchett, R.J., Hall-Spencer, J.M., Milazzo, M., 2015. Physiological advantages of dwarfing in surviving extinctions in high-CO_2 oceans. Nature Climate Change, 5(7), 678–682.

Gillikin, D.P., Lorrain, A., Meng, L., Dehairs, F., 2007. A large metabolic carbon contribution to the $\delta^{13}C$ record in marine aragonitic bivalve shells. Geochim. Cosmochim. Acta 71, 2936-2946.

Gutknecht, J., Bisson, M.J., Tosteson, F.C., 1977. Diffusion of carbon dioxide through lipid bilayer membranes: effects of carbonic anhydrase, bicarbonate, and unstirred layers. J. Gen. Physiol. 55, 1-17.

Hahn, S., Rodolfo-Metalpa, R., Griesshaber, E., Schmahl, W.W., Buhl, D., Hall-Spencer, J.M., Baggini, C., Fehr, K.T., Immenhauser, A., 2012. Marine bivalve shell geochemistry and ultrastructure from modern low pH environments:

724 Environmental effect versus experimental bias. Biogeosciences, 9(5), 1897–1914.
725 Hall-Spencer, J.M., Rodolfo-Metalpa, R., Martin, S., Ransome, E., Fine, M., Turner,
726 S.M., Rowley, S.J., Tedesco, D., Buia, M.C., 2008. Volcanic carbon dioxide vents
727 show ecosystem effects of ocean acidification. Nature 454, 96-99.
728 Hall-Spencer, J.M., Belfiore, G., Tomatsuri, M., Porzio, L., Harvey, B.P., Agostini, S., Kon,
729 K., 2022. Decreased diversity and abundance of marine invertebrates at CO_2
730 seeps in warm-temperate Japan. Zoological Science 39, 41-51.
731 Harvey, B.P., Agostini, S., Wada, S., Inaba, K., Hall-Spencer, J.M., 2018. Dissolution:
732 the Achilles's hell of the triton shell in an acidifying ocean. Front. Mar. Sci. 5, 371.
733 Harvey, B.P., Allen, R., Agostini, S., Hoffmann, L.J., Kon, K., Summerfield, T.C., Wada, S.,
734 Hall-Spencer, J.M., 2021a. Feedback mechanisms stabilise degraded turf algal
735 systems at a CO_2 seep site. Communications Biol. 4, 219.
736 Harvey, B.P., Kerfahi, D., Jung, Y., Shin, J.-H., Adams, J.M., Hall-Spencer, J.M., 2020.
737 Ocean acidification alters bacterial communities on marine plastic debris. Mar.
738 Pollut. Bull. 161, 111749.
739 Harvey, B.P., Kon, K., Agostini, S., Wada, S., Hall-Spencer, J.M., 2021b. Ocean
740 acidification locks algal communities in a species-poor early successional stage.
741 Global Change Biol. 27, 2174-2187.
742 Harvey, B.P., McKeown, N.J., Rastrick, S.P.S., Bertolini, C., Foggo, A., Graham, H., Hall-
743 Spencer, J.M., Milazzo, M., Shaw, P.W., Small, D.P., Moore, P.J., 2016. Individual
744 and population-level responses to ocean acidification. Scientific Reports, 6(1),
745 20194.

He, G., Xiong, X., Peng, Y., Yang, C., Xu, X., Liu, X., Liang, J., Masanja, F., Yang, K., Xu, X., Zheng, Z., Deng, Y., Leung, J.Y.S., Zhao, L., 2023. Transcriptomic responses reveal impaired physiological performance of the pearl oyster following repeated exposure to marine heatwaves. Sci. Total Environ. 854, 158726.

Heinemann, A., Fietzke, J., Melzner, F., Bohm, F., Thomsen, J., Garbe-Schonberg, D., Eisenhauer, A., 2012. Conditions of *Mytilus edulis* extracellular body fluids and shell composition in a pH-treatment experiment: acid-base status, trace elements and $\delta^{11}B$. G-cubed 13.

Higo, S., Callomon, P. and Goto, Y., 1999. Catalogue and Bibliography of the Marine Shell-Bearing Mollusca of Japan. Gastropoda. Bivalvia. Polyplacophora. Scaphopoda, Elle Sci. Publ.

Hughes, T.P., Barnes, M.L., Bellwood, D.R., Cinner, J.E., Cumming, G.S., Jackson, J.B.C., Kleypas, J., van de Leemput, I.A., Lough, J.M., Morrison, T.H., Palumbi, S.R., van Nes, E.H., Scheffer, M., 2017. Coral reefs in the Anthropocene. Nature 546, 82–90.

Hüning, A.K., Melzner, F., Thomsen, J., Gutowska, M.A., Krämer, L., Frickenhaus, S., Rosenstiel, P., Pörtner, H.O., Philipp, E.E.R., Lucassen, M., 2013. Impacts of seawater acidification on mantle gene expression patterns of the Baltic Sea blue mussel: implications for shell formation and energy metabolism. Mar. Biol. 160, 1845-1861.

Inoue, S., Kayanne, H., Yamamoto, S., Kurihara, H., 2013. Spatial community shift from hard to soft corals in acidified water. Nat. Clim. Chang. 3, 683-687.

IPCC, 2013. Summary for policymakers. In: Stocker, T.F., Qin, D., Plattner, G.-K., Tignor, M., Allen, S.K., Boschung, J., Nauels, A., Xia, Y., Bex, V., Midgley, P.M. (Eds.), Climate Change 2013: the Physical Science Basis. Contribution of Working Group I to the Fifth Assessment Report of the Intergovernmental Panel on Climate Change. Cambridge University Press, Cambridge, United Kingdom and New York, NY, USA, pp. 1-30.

Kerfahi, D., Harvey, B.P., Agostini, S., Kon, K., Huang, R., Adams, J.M., Hall-Spencer, J.M., 2020. Responses of intertidal bacterial biofilm communities to increasing pCO_2. Mar. Biotechnol. 22, 727-738.

Lee, T.H., McGill, R.A.R., Fitzer, S., 2021. Effects of extra feeding combined with ocean acidification and increased temperature on the carbon isotope values ($\delta^{13}C$) in the mussel shell. J. Exp. Mar. Biol. Ecol. 541, 151562.

Leung, J.Y.S., Chen, Y., Nagelkerken, I., Zhang, S., Xie, Z., Connell, S.D., 2020a. Calcifiers can adjust shell building at the nanoscale to resist ocean acidification. Small 16, 2003186.

Leung, J.Y.S., Doubleday, Z.A., Nagelkerken, I., Chen, Y., Xie, Z., Connell, S.D., 2019. How calorie-rich food could help marine calcifiers in a CO_2-rich future. Proc. R. Soc. B 286, 20190757.

Leung, J.Y.S., Nagelkerken, I., Russell, B.D., Ferreira, C.M., Connell, S. D., 2018. Boosted nutritional quality of food by CO_2 enrichment fails to offset energy demand of herbivores under ocean warming, causing energy depletion and mortality. Science of the Total Environment, 639, 360–366.

790 Leung, J.Y.S., Russell, B.D., Connell, S.D., 2017. Mineralogical plasticity acts as a
791 compensatory mechanism to the impacts of ocean acidification. Environmental
792 Science & Technology, 51(5), 2652–2659.
793 Leung, J.Y.S., Russell, B.D., Connell, S.D., 2020. Linking energy budget to physiological
794 adaptation: how a calcifying gastropod adjusts or succumbs to ocean
795 acidification and warming. Sci. Total Environ. 715, 136939.
796 Leung, J.Y.S., Zhang, S., Connell, S.D., 2022. Is ocean acidification really a threat to
797 marine calcifiers? A systematic review and meta-analysis of 980+ studies
798 spanning two decades. Small 18, 2107407.
799 Levin, L.A., Hönisch, B., Frieder, C.A., 2015. Geochemical proxies for estimating faunal
800 exposure to ocean acidification. Geochemistry 28, 62-73.
801 Li, S., Liu, C., Huang, J., Liu, Y., Zhang, S., Zheng, G., Xie, L., Zhang, R., 2016.
802 Transcriptome and biomineralization responses of the pearl oyster *Pinctada*
803 *fucata* to elevated pCO_2 and temperature. Sci. Rep. 6, 18493.
804 Liu, Y.W., Aciego, S.M., Wanamaker, A.D., 2015. Environmental controls on the boron
805 and strontium isotopic composition of aragonite shell material of cultured
806 *Arctica islandica.* Biogeosciences 12, 3351-3368.
807 Liu, Y., Sutton, J.N., Ries, J.B., Eagle, R.A., 2020. Regulation of calcification site pH is a
808 polyphyletic but not always governing response to ocean acidification. Sci. Adv.
809 6, eaax1314.
810 Lu, Y., Wang, L., Wang, L., Cong, Y., Yang, G., Zhao, L., 2018. Deciphering carbon
811 sources of mussel shell carbonate under experimental ocean acidification and

812 warming. Mar. Environ. Res. 142, 141-146.
813 Lucas, A., Beninger, P.G., 1985. The use of physiological condition indices in marine
814 bivalve aquaculture. Aquaculture 44, 187-200.
815 Lucey, N.M., Lombardi, C., DeMarchi, L., Schulze, A., Gambi, M.C., Calosi, P., 2015. To
816 brood or not brood: are marine invertebrates that protect their offspring more
817 resilient to ocean acidification? Sci. Rep. 5, 12009.
818 Marin, F., Le Roy, N., Marie, B., 2012. The formation and mineralization of mollusk
819 shell. Front. Biosci. S4, 1099-1125.
820 Martins, M., Carreiro-Silva, M., Martins, G.M., e Ramos, J.B., Viveiros, F., Couto, R.P.,
821 Parra, H., Monteiro, J., Gallo, F., Silva, C., Teodosio, A., Guilini, K., Hall-Spencer,
822 J.M., Leitao, F., Chicharo, L., Range, P., 2021. *Ervilia castanea* (Mollusca, Bivalvia)
823 populations adversely affected at CO_2 seeps in the North Atlantic. Sci. Total
824 Environ. 754, 142044.
825 McConnaughey, T.A., Burdett, J., Whelan, J.F., Paull, C.K., 1997. Carbon isotopes in
826 biological carbonates: respiration and photosynthesis. Geochem. Cosmochim.
827 Acta 61, 611-622.
828 Melzner, F., Mark, F.C., Seibel, B.A., Tomanek, L., 2020. Ocean acidification and
829 coastal marine invertebrates: tracking CO_2 effects from seawater to the cell.
830 Annual Rev. Marine Sci. 12, 499-523.
831 Morton, B., 2019. The biology and functional morphology of *Septifer bilocularis* and
832 *Mytilisepta virgata* (Bivalvia: Mytiloidea) from corals and the exposed rocky
833 shores, respectively, of Hong Kong. Regional Studies in Marine Science 25,

834 100454.
835 Morton, B., Leung, P.T.Y., Wei, J., Lee, G.Y., 2020. A morphological and genetic
836 comparison of *Septifer bilocularis*, *Mytilisepta virgata* and *Brachidontes*
837 *variabilis* (Bivalvia: Mytiloidea) from Hong Kong and erection of the
838 Mytiliseptiferinae sub-fam. nov. Regional Studies in Marine Science 34, 100981.
839 Noisette, F., Comtet, T., Legrand, E., Bordeyne, F., Davoult, D., Martin, S., 2014. Does
840 encapsulation protect embryos from the effects of ocean acidification? The
841 example of *Crepidula fornicata*. PLoS One 9, 1-11.
842 Palmer, A.R., 1992. Calcification in marine molluscs: how costly is it? Proc. Natl. Acad.
843 Sci. U. S. A. 89, 1379-1382.
844 Parker, L.M., O'Connor, W.A., Raftos, D.A., Pörtner, H.O., Ross, P.M., 2015. Persistence
845 of positive carryover effects in oysters following transgenerational exposure to
846 ocean acidification. PloS One 10, e0132276.
847 Pierrot, D.E., Lewis, E., Wallace, D.W.R., 2006. MS Excel Program Developed for CO_2
848 System Calculations, ORNL/CDIAC-105a, Carbon Dioxide Information Analysis
849 Center. Oak Ridge National Laboratory, U.S. Department of Energy, Oak Ridge,
850 Tennessee.
851 Rajan, K.C., Meng, Y., Yu, Z., Roberts, S.B., Vengatesen, T., 2021. Oyster
852 biomineralization under ocean acidification: from genes to shell. Glob. Chang.
853 Biol. 27, 3779-3797.
854 Ramajo, L., Pérez-Léon, E., Hendriks, I.E., Marbà, N., Krause-Jensen, D., Sejr, M.K.,
855 Blicher, M.E., Lagos, N.A., Olsen, Y.S., Duarte, C.M., 2016. Food supply confers

calcifiers resistance to ocean acidification. Sci. Rep. 6, 19374.

Ramesh, K., Yarra, T., Clark, M.S., John, U., Melzner, F., 2019. Expression of calcification- related ion transporters during blue mussel larval development. Ecol. Evol. 9, 7157-7172.

Rastrick, S.S.P., Graham, H., Azetsu-Scott, K., Calosi, P., Chierici, M., Fransson, A., et al., 2018. Using natural analogues to investigate the effects of climate change and ocean acidification on northern ecosystems. ICES J. Mar. Sci. 75, 2299-2311.

Récluz C.A., 1848. Description d'un nouveau genre de coquille bivalve nommé Septifère (Septifer). Rev. Zool. Soc. Cuv. 11, 275-279

Reusch, T.B.H., 2014. Climate change in the oceans: evolutionary versus phenotypically plastic responses of marine animals and plants. Evol. Appl. 7, 104-122.

Ricevuto, E., Vizzini, S., Gambi, M.C., 2015. Ocean acidification effects on stable isotope signatures and trophic interactions of polychaete consumers and organic matter sources at a CO_2 shallow vent system. Journal of Experimental Marine Biology and Ecology 468, 105-117.

Ross, P.M., Parker, L., Byrne, M., 2016. Transgenerational responses of molluscs and echinoderms to changing ocean conditions. ICES J. Mar. Sci. 73, 537-549.

Saleuddin, A.S.M., Petit H.P., 1983. The mode of formation and the structure of the periostracum. In Physiology, Part 1 The Mollusca, vol. 4 (eds. Saleuddin, A.S.M., Wilbur, K.M.). Academic Press, New York, pp. 199-234.

Sheridan, J.A., Bickford, D., 2011. Shrinking body size as an ecological response to

878 climate change. Nat. Clim. Change 1, 401-406.
879 Sillanpää, J.K., Sundh, H., Sundell, K.S., 2018. Calcium transfer across the outer
880 mantle epithelium in the Pacific oyster, Crassostrea gigas. Proc. R. Soc. B 285,
881 20181676.
882 Spalding, C., Finnegan, S., Fischer, W.W., 2017. Energetic costs of calcification under
883 ocean acidification. Global Biogeochem. Cycles 31, 866-877.
884 Thomsen, J., Stapp, L.S., Haynert, K., Schade, H., Danelli, M., Lannig, G., Wegner, K.M.,
885 Melzner, F., 2017. Naturally acidified habitat selects for ocean acidification-
886 tolerant mussels. Sci. Adv. 3, e1602411.
887 Waldbusser, G.G., Brunner, E.L., Haley, B.A., Hales, B., Langdon, C.J., Prahl, F.G., 2013.
888 A developmental and energetic basis linking larval oyster shell formation to
889 acidification sensitivity. Geophys. Res. Lett. 40, 2171-2176.
890 Waldbusser, G.G., Hales, B., Langdon, C.J., Haley, B.A., Schrader, P., Brunner, E.L., Gray,
891 M.W., Miller, C.A., Gimenez, I., 2014. Saturation-state sensitivity of marine
892 bivalve larvae to ocean acidification. Nat. Clim. Change 5, 273-280.
893 Waldbusser, G.G., Gray, M.W., Hales, B., Langdon, C.J., Haley, B.A., Gimenez, I., Smith,
894 S.R., Brunner, E.L., Hutchinson, G., 2016. Slow shell building, a possible trait for
895 resistance to the effects of acute ocean acidification. Limnol. Oceanogr. 61,
896 1969-1983.
897 Witkowski, C. R., Agostini, S., Harvey, B. P., van der Meer, M. T. J., Sinninghe Damsté, J.
898 S., Schouten, S., 2019. Validation of carbon isotope fractionation in algal lipids as
899 a pCO_2 proxy using a natural CO_2 seep (Shikine Island, Japan). Biogeosciences,

16, 4451–4461.

Wikelski, M., Thom, C., 2000. Marine iguanas shrink to survive El Nino. Nature 403, 37-38.

Zhao, L., Liu, B., An, W., Deng, Y., Lu, Y., Liu, B., Wang, L., Cong, Y., Sun, X., 2019a. Assessing the impact of elevated pCO_2 within and across generations in a highly invasive fouling mussel (*Musculista senhousia*). Sci. Total Environ. 689, 322-333.

Zhao, L., Lu, Y., Yang, F., Liang, J., Deng, Y., 2020b. Transgenerational biochemical effects of seawater acidification on the Manila clam (*Ruditapes philippinarum*). Sci. Total Environ. 710, 136420.

Zhao, L., Milano, S., Walliser, E.O., Schöne, B.R., 2018b. Bivalve shell formation in a naturally CO_2-enriched habitat: unraveling the resilience mechanisms from elemental signatures. Chemosphere 203, 132-138.

Zhao, L., Schöne, B.R., Mertz-Kraus, R., Yang, F., 2017a. Insights from sodium into the impacts of elevated pCO_2 and temperature on bivalve shell formation. J. Exp. Mar. Biol. Ecol. 486, 148-154.

Zhao, L., Schöne, B.R., Mertz-Kraus, R., Yang, F., 2017b. Sodium provides unique insights into transgenerational effects of ocean acidification on bivalve shell formation. Sci. Total Environ. 577, 360-366.

Zhao, L., Shirai, K., Tanaka, K., Milano, S., Higuchi, T., Murakami-Sugihara, N., Walliser, E.O., Yang, F., Deng, Y., Schöne, B.R., 2020a. A review of transgenerational effects of ocean acidification on marine bivalves and their implications for sclerochronology. Estuar. Coast. Shelf S., 235, 106620.

922 Zhao, L., Shirai, K., Murakami-Sugihara, N., Higuchi, T., Tanaka, K., 2019b. Mussel
923 periostracum as a high-resolution archive of soft tissue δ13C records in coastal
924 ecosystems. Geochem. Cosmochim. Acta 260, 232-243.
925 Zhao, L., Yang, F., Milano, S., Han, T., Walliser, E.O., Schöne, B.R., 2018a.
926 Transgenerational acclimation to seawater acidification in the Manila clam
927 *Ruditapes philippinarum*: preferential uptake of metabolic carbon. Sci. Total
928 Environ. 627, 95-103.
929 Zhao, L., Yang, F., Yan, X., 2013. Stable isotopes and fatty acids as dietary tracers of
930 intertidal bivalves. Fisheries Sci. 79, 749-756.

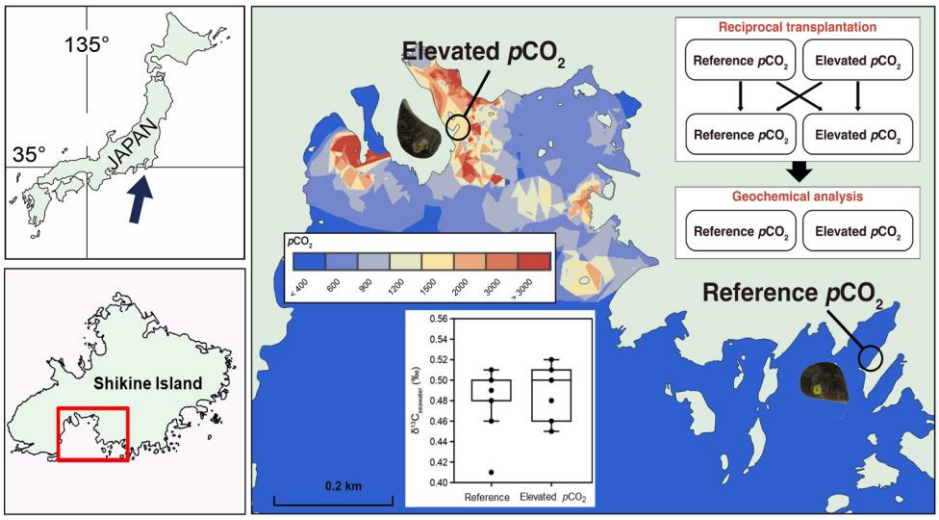

Figure 1 Volcanic CO_2 seeps off Shikine Island (Japan) showing the spatial variability in seawater pCO_2 (based on data by Agostini et al. 2018 using ArcGIS 10.2 software) and the average $\delta^{13}C$ ratio of seawater DIC near and outside the CO_2 seeps (based on data collected during the survey in October 2019). Experimental design showing reciprocal transplantation and high-resolution analysis of shell geochemistry of mussels (*Septifer bilocularis*) collected from the reference and elevated pCO_2 sites. Mussels were labelled with a reference number using queen bee marking tags for identification.

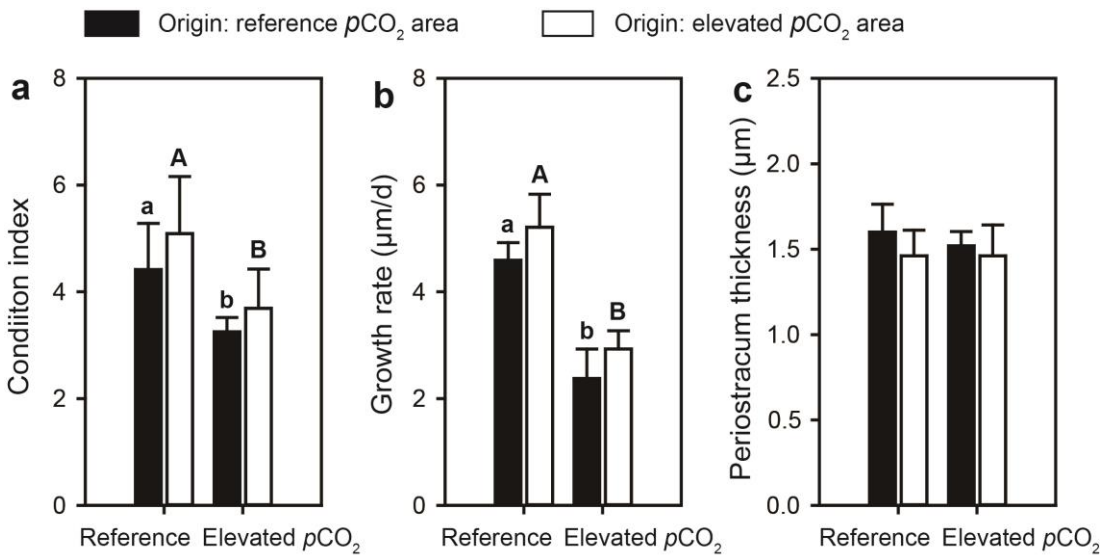

942

943 **Figure 2** Growth performance of mussels collected from the reference pCO_2 and

944 elevated pCO_2 areas following reciprocal transplantation. (a) condition index; (b)

945 growth rate; (c) the thickness of periostracum. Solid black fill indicates that

946 individuals originated from reference pCO_2 area, and solid white fill indicates that

947 individuals originated from elevated pCO_2 area. Small letters indicate a significant

948 difference in mussels originating from the reference pCO_2 area under reference and

949 elevated pCO_2 conditions, and capital letters indicates significant differences in those

950 mussels originally collected from the elevated pCO_2 area.

951

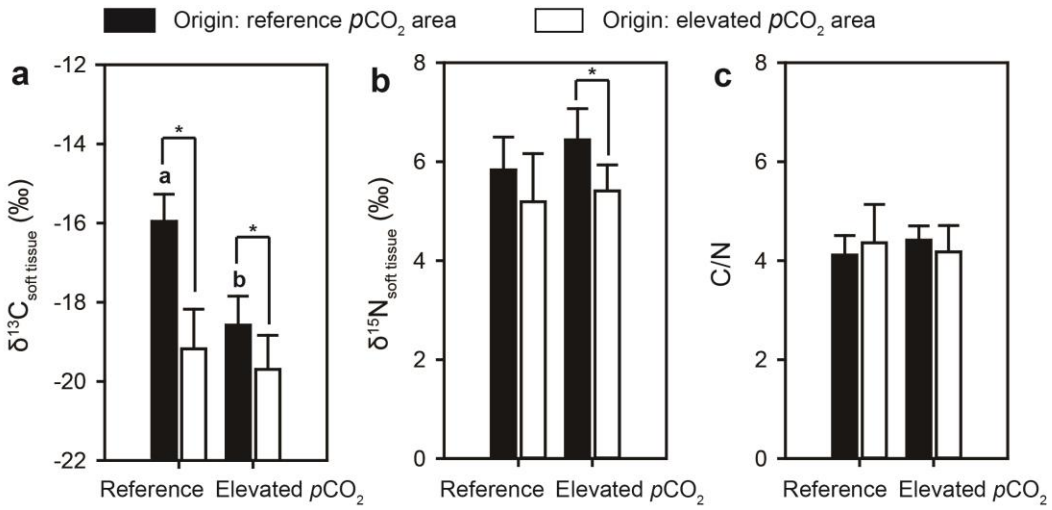

952

953 **Figure 3** Somatic stable isotopic signatures of mussels from the reference pCO_2 and
954 elevated pCO_2 areas following reciprocal transplantation. (a) stable carbon isotope
955 ($\delta^{13}C$); (b) stable nitrogen isotope ($\delta^{15}N$); (c) C/N. Small letters indicate a significant
956 difference in mussels collected from the reference pCO_2 area under low and high
957 pCO_2 conditions, and an asterisk indicates a significant difference between
958 reciprocally transplanted mussels subjected to the same pCO_2 scenario.

959

960

961

962

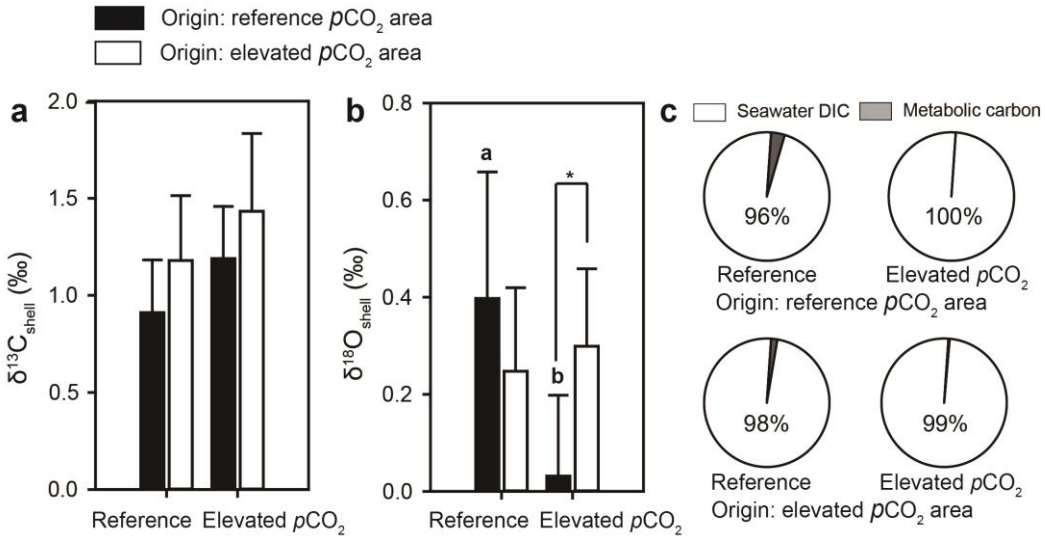

963

964 **Figure 4** Shell geochemical properties of mussels from the reference pCO_2 and

965 elevated pCO_2 areas following reciprocal transplantation. (a) stable carbon isotope

966 ($\delta^{13}C$); (b) stable oxygen isotope ($\delta^{18}O$); (c) relative contribution of seawater DIC and

967 metabolic carbon to shell carbonate. Small letters indicate a significant difference in

968 mussels collected from the reference pCO_2 area under low and high pCO_2 conditions,

969 and an asterisk indicates a significant difference between reciprocally transplanted

970 mussels subjected to the same pCO_2 scenario.

971

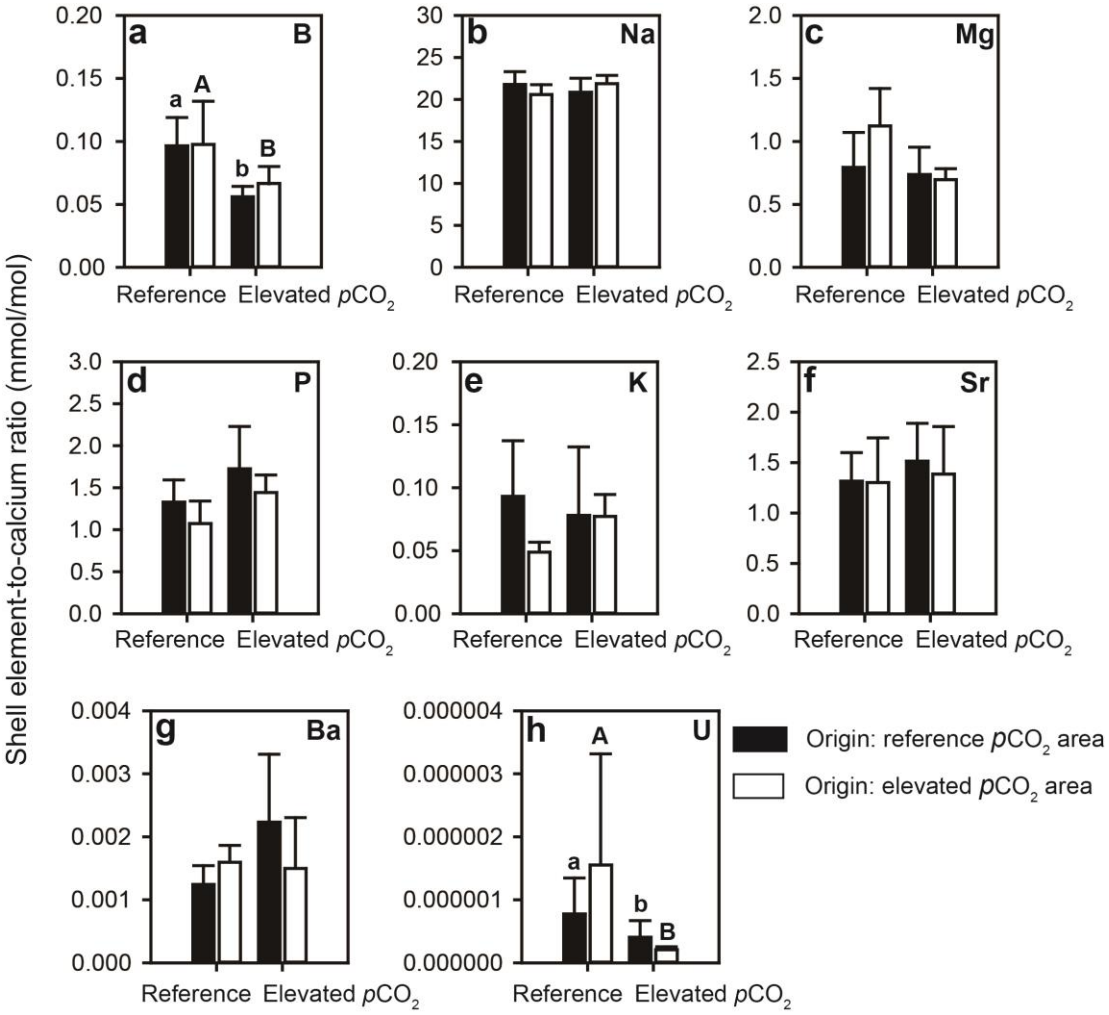

Figure 5 Shell element-to-calcium ratios of mussels collected from the reference pCO_2 and elevated pCO_2 areas following reciprocal transplantation. (a) B/Ca; (b) Na/Ca; (c) Mg/Ca; (d) P/Ca; (e) K/Ca; (f) Sr/Ca; (g) Ba/Ca; (h) U/Ca. Small letters indicate a significant difference in mussels originating from the reference pCO_2 area under reference and elevated pCO_2 conditions, and capital letters indicates significant differences in those mussels originally collected from the elevated pCO_2 area.

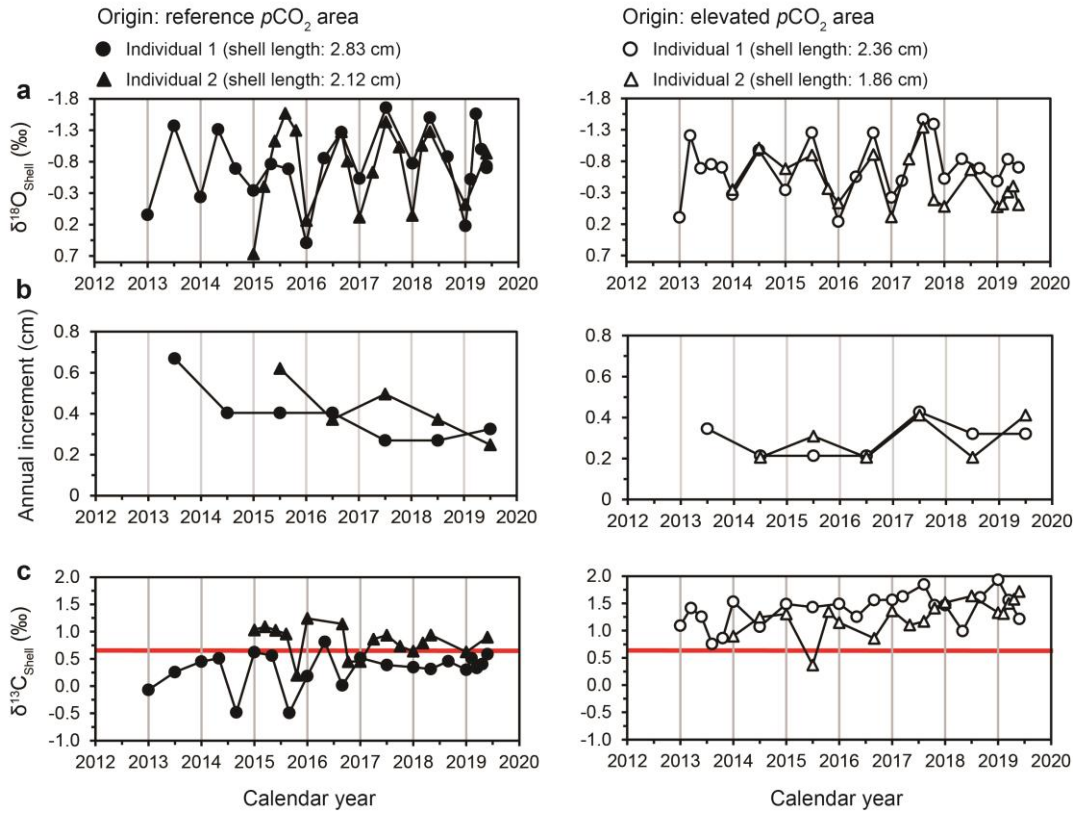

Figure 6 Analysis of shell geochemistry in mussels collected from the reference pCO_2 and elevated pCO_2 areas. Two individuals were selected from the reciprocal transplant experiment for further analysis. This used only those procedural control individuals that had been collected from, and transplanted back into the same site. (a) stable oxygen isotope ($\delta^{18}O$) of mussel shells according to which each shell portion was placed into a temporal context and ontogenetic age of each mussel was then determined; (b) annual increment calculated according to the temporal aligned shell portion; (c) stable carbon isotope ($\delta^{13}C$) of mussel shells. Red lines indicate the mean $\delta^{13}C$ ratio of seawater DIC in the reference pCO_2 and elevated pCO_2 areas.